Environmental Science
Processes & Impacts

Towards a Comprehensive Understanding of Malathion Degradation: Comparison of Degradation Reactions under Alkaline and Radical Conditions

Journal:	*Environmental Science: Processes & Impacts*
Manuscript ID	EM-ART-02-2022-000050.R1
Article Type:	Paper

Malathion is a commercial organophosphate insecticide which functions as an acetylcholinesterase inhibitor. Both this organophosphate compound and its mechanism of action are common across many pesticide compounds. Research has shown how malathion degrades in the environment. Several degradation techniques for malathion involve generation of OH• radicals; however these studies typically examine only the disappearance of malathion, and not the subsequent degradation of breakdown products (some of which are also toxic). Our computational data demonstrate that OH• is only effective for degradation at certain steps along the complete pathway, whereas OH^- ion may be more effective in others. These findings suggest that variable reaction conditions could be employed for a more complete degradation process for malathion and similar organophosphorus compounds.

Towards a Comprehensive Understanding of Malathion Degradation: Comparison of Degradation Reactions under Alkaline and Radical Conditions

*Robert W. Lamb[1,2], Harley McAlexander[3], Christa M. Woodley[3], and Manoj K. Shukla[3]**

[1]Oak Ridge Institute for Science and Education, Oak Ridge, TN, USA

[2]Current affiliation: Simetri Inc., 7005 University Blvd, Winter Park, FL 32792, USA

[3]US Army Engineer Research and Development Center, Environmental Laboratory, 3909 Halls Ferry Road, Vicksburg, MS 39180, USA

ABSTRACT

Malathion is a commercially available insecticide that functions by acting as an acetylcholinesterase inhibitor. Of significant concern, if left in the environment, some of the products observed from the degradation of malathion can function as more potent toxins than the parent compound. Accordingly, there are numerous studies revolving around possible degradation strategies to remove malathion from various environmental media. One of the possible approaches is the degradation of malathion by OH• radicals which could be produced from both artificial and biological means in the environment. While there is plenty of evidence that OH• does in fact degrade malathion, there is little understanding of the underlying mechanism by which OH• reacts with malathion. Moreover, it is not known how competitive the

radical degradation pathway is with analogous alkaline degradation pathways. Even less is known about the reaction of additional OH• radicals with the degradation byproducts themselves. Herein, we demonstrate that OH• induced degradation pathways have variable competitiveness with OH^- driven degradation pathways and, in some cases, produce quite different reactivity.

KEYWORDS: Malathion, cholinesterase inhibitor, DFT, degradation kinetics, environmental fate

*Corresponding author; email: Manoj.K.Shukla@usace.army.mil

INTRODUCTION

Organophosphorus compounds (OPCs) are commonly found in herbicides, pesticides, and chemical warfare agents for much the same reason: they act as potent acetylcholinesterase inhibitors. From an environmental perspective, the accumulation of OPCs in the environment can negatively affect human health.[1] One such OPC, malathion, is used worldwide for pest control on a variety of crops.[2] Due to its widespread utilization and potential for toxicity as an OPC, extensive experimental studies have been conducted under various conditions on the degradation of malathion, the pesticide's effects on microbes and animals,[3-5] and the development and application of chemical or biological remediation techniques.[4, 6-21]

In our previous study, we demonstrated that under alkaline conditions, the initial degradation products of malathion can break down further under those same conditions.[22] In some instances, the secondary or even tertiary breakdown products were known themselves to be toxic.[23] There

are several degradation studies that involve radical mechanisms, typically with OH• radical being directly implicated.[7, 12, 18, 24-26] Various techniques involving TiO_2 have been reported examining different aspects of the radical generation process including alloy composition,[12] doping,[18] and synergistic effects with ozone,[7, 24] although in each case the overall objective is to generate OH• from irradiation of TiO_2. Others have explored stimulating Photosystem II in algae,[25] or even using graphitic carbon nitride as photocatalysts.[26]

While these degradation techniques have been studied for the removal of malathion, there is little work in the literature on the underlying degradation mechanism involving OH• radical, which would be useful for creating more effective remediation strategies. Yu and coworkers[12] provided a short discussion on a potential photocatalytic mechanism, but this discussion is focused on the alteration of the TiO_2 surface to reduce recombination of the photoelectrons with their holes and not on the interaction of the generated OH• radicals with malathion. Nicodemus and coworkers[25] noted that hydrolysis of malathion by OH• under light conditions appears to occur primarily through a nucleophilic attack mechanism. Indeed, there is literature precedent for OH• reacting in this manner. De Vleeschouwer and coworkers[27] determined that several radicals relevant to organic chemistry (including OH•) can demonstrate either electrophilic or nucleophilic character. Furthermore, Pari and coworkers published a computational study in 2017 demonstrating that OH• can act as a nucleophile if an appropriate electrophilic site is present on aromatic systems.[28]

Unfortunately, a similar mechanistic study has yet to be extended to malathion. Further, in most of these studies[7, 12, 18, 24-26] it is implied that the OH• radical is generated by an interaction of an OH^- ion with the TiO_2 surface. If an OH^- ion is already present in the solution, there is a possibility that malathion could have already undergone partial degradation to some of its myriad

products. Because of this possible competition in reactivity, there is a need to compare the alkaline and radical degradation mechanisms at multiple steps along the degradation pathway. From this analysis we will be able to ascertain if alkaline or radical degradation is preferred at any particular step. If a particular pathway is dominant, then designing remediation strategies becomes more straightforward. On the other hand, if it is found that different pathways are favored under different conditions, then this could inform the design of potential tandem remediation strategies, *e.g.* processes are designed wherein the degradation products are subsequently treated under different conditions than the degradation of the parent compound. To that end, herein we examine the radical degradation pathways of malathion and several of its plausible alkaline degradation products from our previous publication.

COMPUTATIONAL DETAILS

All computations were performed using the C.01 Revision of the Gaussian 16 suite of programs.[29] All geometries were optimized with the M06-2X density functional,[30] the 6-31G(d,p) basis set (employing cartesian d functions),[31-33] and the IEFPCM implicit solvation model[34-54] using parameters consistent with water as the solvent. Additionally, explicit water molecules were also used (except where noted) to stabilize the hydroxide ion or hydroxyl radical and facilitate the optimization of intended species and transition states. For computational simplicity, all ethyl groups were truncated to methyl groups. Optimized geometries were confirmed to be minima or transition states by a subsequent analytical frequency computation yielding 0 (minimum) or 1 (transition state) imaginary modes at the same level of theory. Transition states were also validated by connecting to respective reactants and products through

the displacement of the TS geometry along the vector of the imaginary mode. The resulting geometries of reactants and products obtained through this procedure were again fully optimized to ensure their correctness. More reliable energies were obtained using single-point energy computations with the more robust aug-cc-pVTZ[55, 56] basis set. Free energies at these single-point energy computations were obtained by applying the thermodynamic corrections from the M06-2X/6-31G(d,p) level of theory. The mechanistic discussion will use the relative energies from M06-2X/aug-cc-pVTZ//M06-2X/6-31G(d,p) level of theory. M06-2X is considered to provide reasonable thermodynamic data,[30] is consistent with prior literature (*vide infra*) in using a triple-ζ basis set and is a fraction of the expense of analogous post-HF MP2 computations. For completeness of data relative to prior literature, post-HF *ab initio* MP2 computations[57-61] (MP2/aug-cc-pVTZ//M06-2x/6-31G(d,p)) were also performed and the analogous data are available in the Supporting Information (SI) section. Overall, the trends in the data from MP2 computations are qualitatively consistent with the M06-2X results, although the specific may be quite different. MP2 overestimating barrier heights is a known issue in the literature[28, 62] and thus the data from MP2 should only be considered with caution and with respect to prior literature on this subject. Reaction timescales were determined by converting the computed free energy of activation to a rate constant via the Eyring equation (Equation 1)

$$k = \frac{k_B T}{h} e^{-\frac{\Delta G^{\ddagger}}{RT}}$$

where $\Delta G^{\ddagger}$ is the Gibbs free energy of activation, k_B is Boltzmann's constant, and h is Planck's constant.

RESULTS AND DISCUSSION

A common mechanism for malathion degradation is elimination by hydroxide ion (Figure 1, black) to yield diethyl fumarate and a dithiophosphate, **2**. Similarly, H• abstraction by hydroxyl radical (Figure 1, red) is also highly exergonic, albeit not as significantly as the reaction with a hydroxide ion. However, after H• abstraction the C-S remains intact with a radical electron residing the ß carbon, **3**. While the bond is intact, this new radical species is likely quite fragile and will continue to degrade through additional pathways. Additionally, the transition state energies between these two reaction pathways are both quite low at 3.5 and 4.6 kcal mol^{-1} for hydroxide ion and hydroxyl radical, respectively. These data demonstrate that generating radicals or alkaline conditions will be suitable to facilitate this degradation pathway.

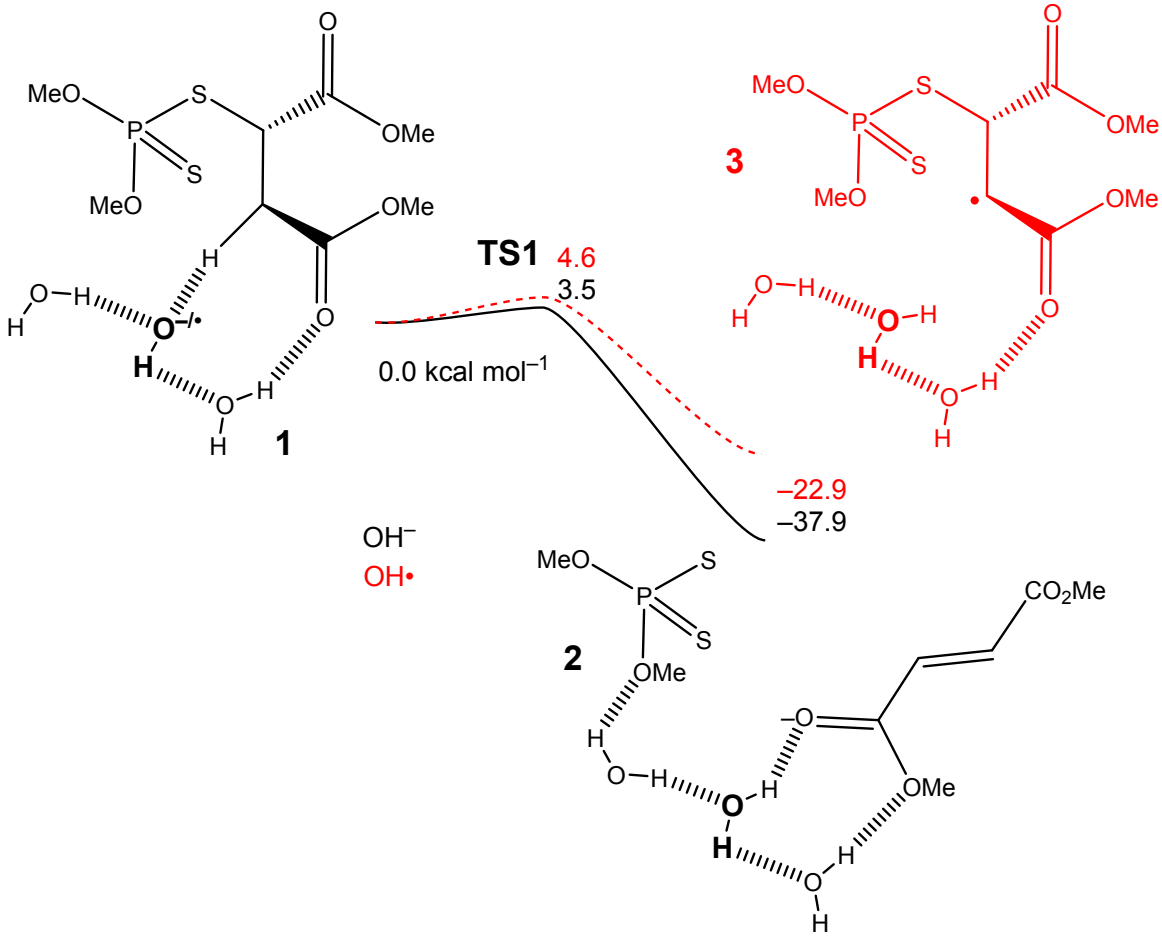

Figure 1. Hydroxide- vs. hydroxyl radical-assisted elimination reactions of malathion at the M06-2X/aug-cc-pVTZ//M06-2X/6-31G(d,p) level of theory in bulk water. Non-bolded numbers indicate relative free energies in kcal mol^{-1}. Bolded numbers denote the compound numbers as local minimum (standard) or transition state (leading "TS") geometries. Atoms corresponding to the hydroxide ion or hydroxyl radical are bolded and enlarged throughout the reaction. The position of the negative charge or radical electron are also noted when localized to a single atom.

Additional considerations must be made for the possibility of subsequent and/or alternative reaction pathways. In our previous publication,[22] we found that the hydroxide ion was able to

react at multiple sites, and additional hydroxide ions could then continue to react to bring about secondary and tertiary products, some of which were found to be toxic by other research groups.[23] Similar mechanistic pathways should be considered for reactions with hydroxyl radicals. Because diethyl fumarate has been shown to be toxic to aquatic life,[23] its degradation pathway via OH^- was also compared to OH• and the results are shown in Figure 2. A proximal OH• attacks a carbonyl carbon of **4** creating tetrahedral intermediate **5**. While the association is slightly endergonic (5.4 kcal mol^{-1}), subsequent loss of a methoxyl radical to generate monoacid **6** is reasonably exergonic (–13.7 kcal mol^{-1}). With OH^-, **6** would rapidly deprotonate to form the methanol and a carboxylate, **7**. However, in the OH• sequence, the protonated structure **6**, with a proximal methoxy radical is more stable than the carboxyl radical structure **7**. Additionally, **TS2** and **TS3** are notably higher in energy ($\Delta\Delta G^{\ddagger}$ = +10.8 and +7.0 kcal mol^{-1}, respectively) for the OH• pathway than OH^-. Given these data, degradation of diethyl fumarate by OH• is expected to be significantly slower (reaction time scale of 1.80 s and 0.05 s) than with OH^- (reaction time scale of 2.18×10^{-8} s and 3.84×10^{-7} s) , albeit still plausible. It should be noted that the degradation pathways in Figure 2 do not connect directly to those in Figure 1. Rather, Figure 2 assumes that malathion was previously degraded to dimethyl fumarate by an OH^- hydrolysis as shown in Figure 1, byproducts have dissipated into solution, and the remaining compound can now be degraded further by either additional OH^- or OH•. This break between reaction steps is intentional and is done throughout the text to better focus on the differences between OH^- and OH• for a particular reaction step.

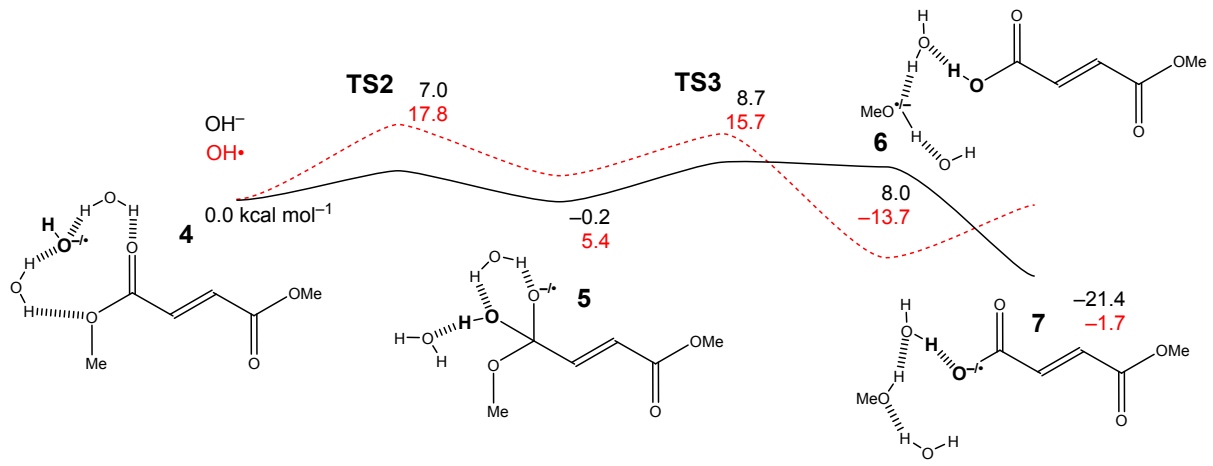

Figure 2. Sequential hydrolysis of A) dimethyl fumarate to methyl fumarate at the M06-2X/aug-cc-pVTZ//M06-2X/6-31G(d,p) level of theory in bulk water. Non-bolded numbers indicate relative free energies in kcal mol^{-1}. Bolded numbers denote the compound numbers as local minimum (standard) or transition state (leading "TS") geometries. Atoms corresponding to the hydroxide ion or hydroxyl radical are bolded and enlarged throughout the reaction. The position of the negative charge or radical electron are also noted when localized to a single atom.

Following the sequence in Figure 2, the MeOH byproduct can migrate away from methyl fumarate and be replace by an additional OH$^-$ or OH•. The subsequent degradation of methyl fumarate **7** by OH• was computed and compared to degradation by OH$^-$ and the resulting data are shown in Figure 3. In the sequence in Figure 3, a proximal OH• attacks a carbonyl carbon of **8** creating tetrahedral intermediate **9**. This association is significantly more endergonic than the association in the previous step at 15.6 kcal mol^{-1} (vs 5.4 kcal mol^{-1} in Figure 2), although subsequent loss of a methoxyl radical to generate **10** still makes the process overall exergonic at –8.5 kcal mol^{-1}. Again, with OH$^-$ structure **10** would rapidly deprotonate to **11**, whereas with OH•, structure **10** with a proximal methoxy radical is more stable than **11** with a carboxyl

radical. Additionally, **TS4** and **TS5** are again notably higher in energy ($\Delta\Delta G^{\ddagger}$ = +9.3 and +8.4 kcal mol^{-1}, respectively) for the OH• pathway than OH^{-}. Moreover, **TS4** and **TS5** are even higher than **TS2** and **TS3**, respectively. Given these data, degradation of methyl fumarate by OH• is plausible, albeit rather unlikely to occur (**TS4** timescale of 122 s vs 1.86×10^{-5} s for OH• and OH^{-}, respectively) relative to other degradation processes (i.e. OH^{-}) due to the significant increase in the transition state energies.

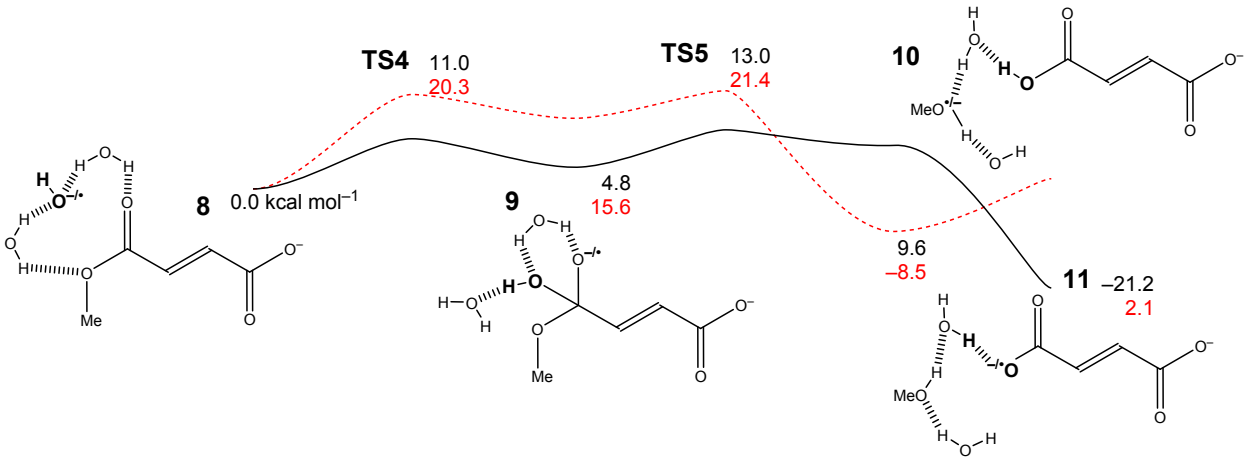

Figure 3. Sequential hydrolysis of methyl fumarate to fumarate at the M06-2X/aug-cc-pVTZ//M06-2X/6-31G(d,p) level of theory in bulk water. Non-bolded numbers indicate relative free energies in kcal mol^{-1}. Bolded numbers denote the compound numbers as local minimum (standard) or transition state (leading "TS") geometries. Atoms corresponding to the hydroxide ion or hydroxyl radical are bolded and enlarged throughout the reaction. The position of the negative charge or radical electron are also noted when localized to a single atom.

After hydrolysis to fumarate, the olefin can react further to malate as shown in Figure 4. Again, the MeOH byproduct from Figure 3 is first replaced by an additional OH^- or OH• to yield **12**. The association of OH^- to **12** via **TS6** is quite endergonic ($\Delta G^{\ddagger}$ = 27.9 kcal mol^{-1}). Although subsequent steps make hydrolyzing the double bond exergonic overall, products **14** and **15** are unlikely to be observed experimentally under alkaline conditions. However, the association of OH• to **12** is quite facile ($\Delta G^{\ddagger}$ = 5.3 kcal mol^{-1}). The resulting **13** can react further to complete the generation of malate and the regeneration of an OH• radical and **14**. In the sequence from **12** to **14**, OH• is effectively catalytic. Following this sequence, there is a possibility for the OH• to migrate from the carboxyl group of **14** to the OH group of **16**. From **16**, the OH• radical can abstract an H atom through a facile **TS8**, to generate a partially decarboxylated structure **17** (Figure 4) in which the unpaired electron is delocalized between the two fragments. It is feasible that CO_2 would be fully liberated from this structure thus resulting in degradation of malate.

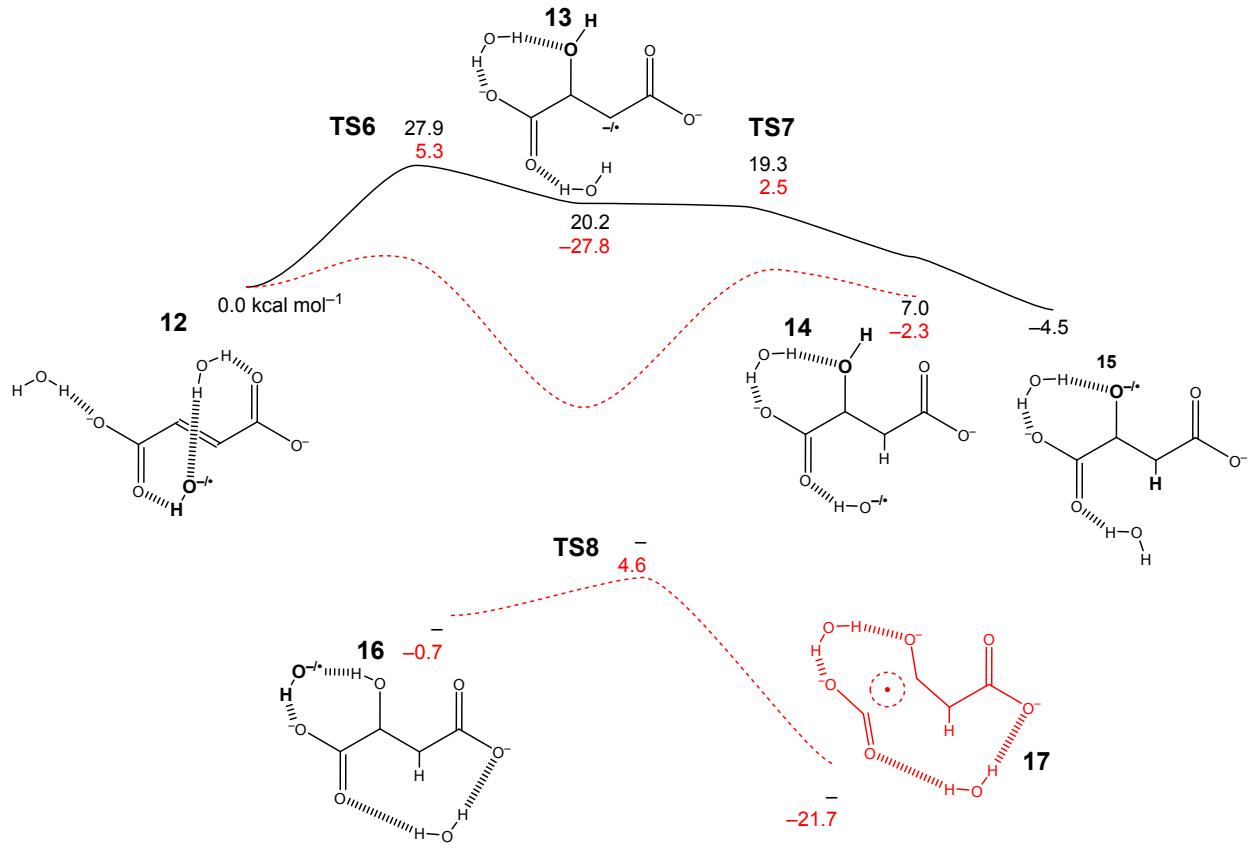

Figure 4. A) Fumarate to malate (**12** → **15**) and B) decarboxylation of malate (**16** → **17**) at the M06-2X/aug-cc-pVTZ//M06-2X/6-31G(d,p) level of theory in bulk water. Non-bolded numbers indicate relative free energies in kcal mol^{-1}. Bolded numbers denote the compound numbers as local minimum (standard) or transition state (leading "TS") geometries. Atoms corresponding to the hydroxide ion or hydroxyl radical are bolded and enlarged throughout the reaction. The position of the negative charge or radical electron are also noted when localized to a single atom.

At each reaction step, hydrolysis of the OMe groups of fumarate by OH• will be significantly slower than with OH^- (**TS2**, **TS3**, **TS4**, **TS5**). However, breaking the double bond of fumarate to form malate (**TS6** and **TS7**) is prohibitively high in energy with OH^- (**TS6** timescale of 4.55×10^7

s) but is quite facile with OH• (**TS6** timescale of 1.24×10^{-9} s). Additionally, OH• can further degrade malate. Structure **17** shows the partial decarboxylation with the unpaired electron delocalized between the C and O atoms of the two fragments. Despite repeated attempts, an analogous transition state with OH^- was not located for **TS8**. These data demonstrate that, although plausible, under radical degradation conditions, diethyl fumarate is much less likely to degrade by a hydrolysis-like mechanism. Conversely, if the fumarate dianion is already generated from another degradation process, it can undergo an additional degradation and potentially decarboxylation step via OH• that is not readily available with OH^-. These data indicate that variable treatment methodologies could be employed to effeciently remove not only the initial contaminant, but also the degradation products.

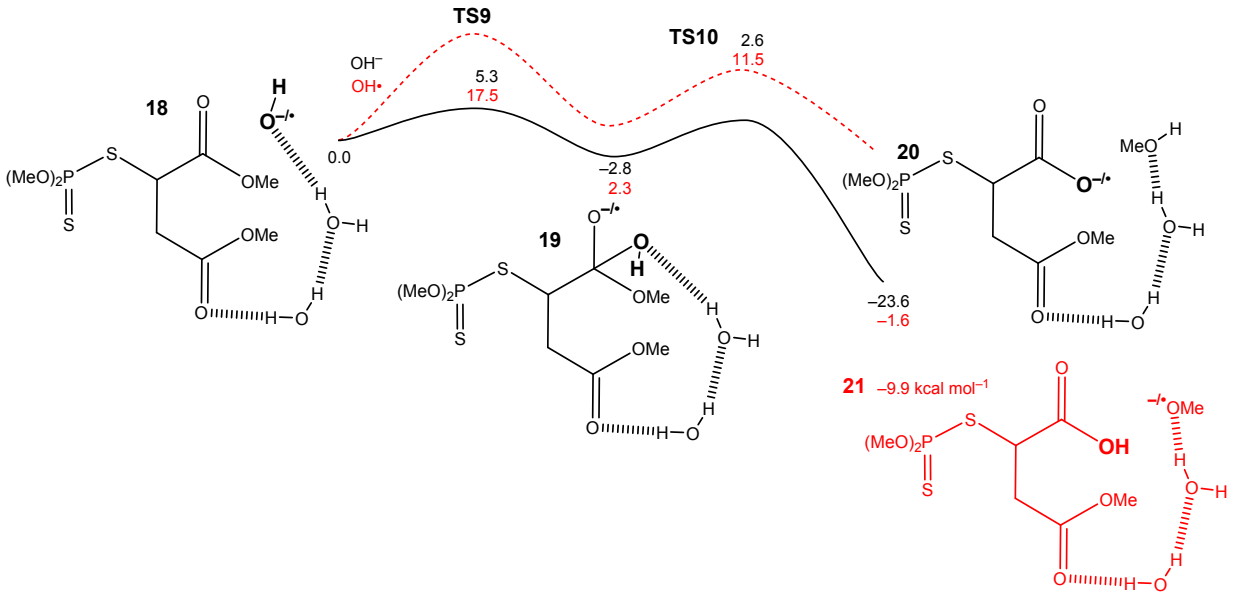

Figure 5. Initial α-ester degradation at the M06-2X/aug-cc-pVTZ//M06-2X/6-31G(d,p) level of theory in bulk water. Non-bolded numbers indicate relative free energies in kcal mol^{-1}. Bolded numbers denote the compound numbers as local minimum (standard) or transition state (leading

"TS") geometries. Atoms corresponding to the hydroxide ion or hydroxyl radical are bolded and enlarged throughout the reaction. The position of the negative charge or radical electron are also noted when localized to a single atom.

In addition to the elimination type reaction and its degradation products shown in Figures 1-4, the ester groups can be hydrolyzed first.[63] The data in Figure 5 show OH^- or OH• initially attacking the ester at the α position relative to the S of the phosphate group. We find that with OH^- the degradation is both facile (**TS9** timescale of 1.24×10^{-9} s) and quite exergonic. However, with OH•, the initial association, **TS9**, is quite endergonic ($\Delta G^{\ddagger}$ = 17.5 kcal mol^{-1}, timescale of 1.08 s) with a mildly endergonic intermediate **19**. The subsequent dissociation of an OMe•, **TS10**, has a lower free energy of activation than the association step, indicating that if **19** is formed, **20** will almost certainly be formed. Once **20** is formed, the dissociated methoxy group picks up an H atom from a neighboring water molecule effectively regenerating the OH• radical. However, in a similar vein to dimethyl fumarate degradation (Figure 2), it is lower in energy for the carboxyl group to retain the H atom and to have a proximal MeO• radical, **21** (in red). Although, once the OMe• migrates away in bulk solution, the carboxyl group will likely become deprotonated again.

After the α site is hydrolyzed, and exchange of the MeOH byproduct for an additional OH^- or OH•, the ß site can react next as shown in Figure 6. Both the association of an OH^- to the ß site, **TS11**, and dissociation of a OMe group, **TS12**, are slightly higher than their counterparts (**TS9** and **TS10** in Figure 5), indicating that hydrolysis of the second ester group will be slower than the first. These results are qualitatively similar if the order is reversed (i.e. ß then α, compounds **25**–**32** in Figures S1 and S2 in the Supporting Information). Association of an OH• to the ß

position, **TS11**, is also higher than at the α position, **TS9**. However, the dissociation of the OMe group via **TS12** is prohibitively high in energy with a free energy of activation of 30.6 kcal mol^{-1} (timescale of 4.33×10^{9} s). These data indicate that once the α position has been degraded, the ß position will not degrade with OH•. Conversely, both the ß and α positions can be degraded by OH•, but only if the ß position reacts first (see Supporting Information). Overall, the degradation of the α or ß ester positions of malathion by OH• is plausible, but significantly slower than degradation by OH^{-}

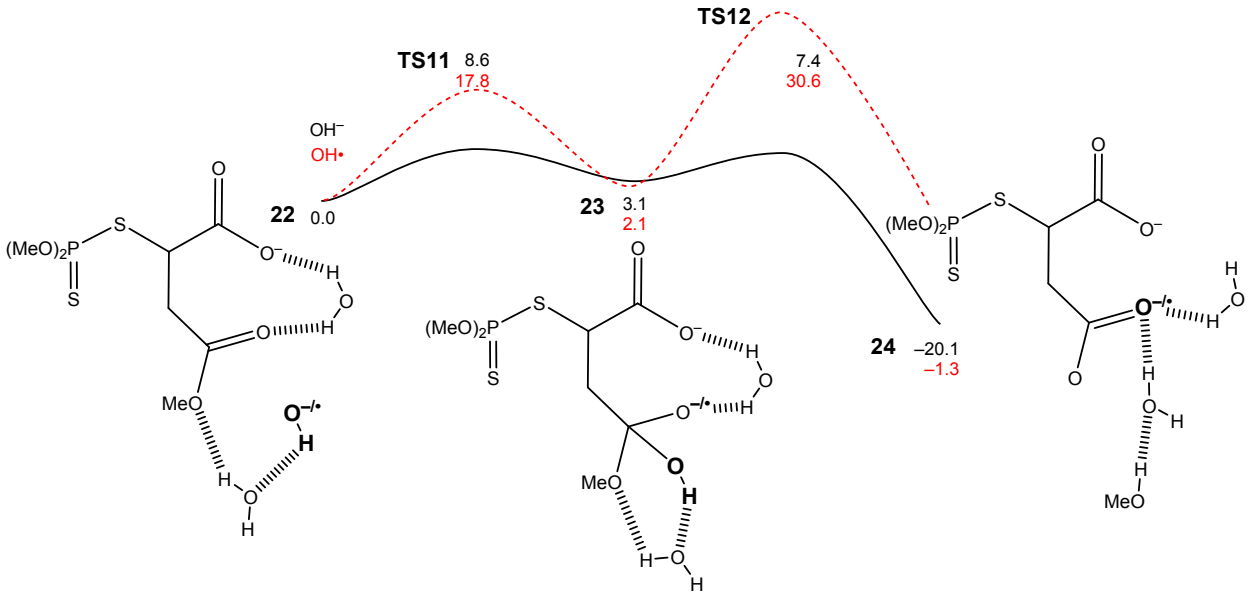

Figure 6. ß-ester degradation following α-ester hydrolysis at the M06-2X/aug-cc-pVTZ//M06-2X/6-31G(d,p) level of theory in bulk water. Non-bolded numbers indicate relative free energies in kcal mol^{-1}. Bolded numbers denote the compound numbers as local minimum (standard) or transition state (leading "TS") geometries. Atoms corresponding to the hydroxide ion or hydroxyl radical are bolded and enlarged throughout the reaction. The position of the negative charge or radical electron are also noted when localized to a single atom.

While the degradation of the ester groups are quite slow via OH• radical, it is quite facile under alkaline conditions. Once the ester groups have been hydrolyzed by either method, and the byproduct MeOH replaced with an additional OH^- or OH•, the phosphate group can still be reactive as shown in Figure 7. With an OH^- ion this degradation is a multistep process wherein the OH^- ion first associates to **33** to generate a 5-coordinate intermediate **34**. This intermediate then reorganizes and subsequently breaks the P-S bond (**35** → **36**). However, this reaction sequence is quite different with OH• radical. The free energy of activation for association of OH• is significantly higher than OH^- (15.6 vs 6.2 kcal mol^{-1}). Passing through **TS17** generates intermediate **37** (in red), however once the 5-coordinate intermediate has been generated, the unpaired electron reorganizes to be located on the alkyl chain which prompts decarboxylation at the α position. This decarboxylation is quite similar to when fumarate dianion is subjected to an additional radical reaction (see **16→17** in Figure 4), albeit significnaly slower (timescale of 4.38×10^{-2} s vs 5.64×10^{-9} s for OH• and OH^-, respectively) due to the higher energy transition state (15.6 vs 4.6 kcal mol^{-1}).

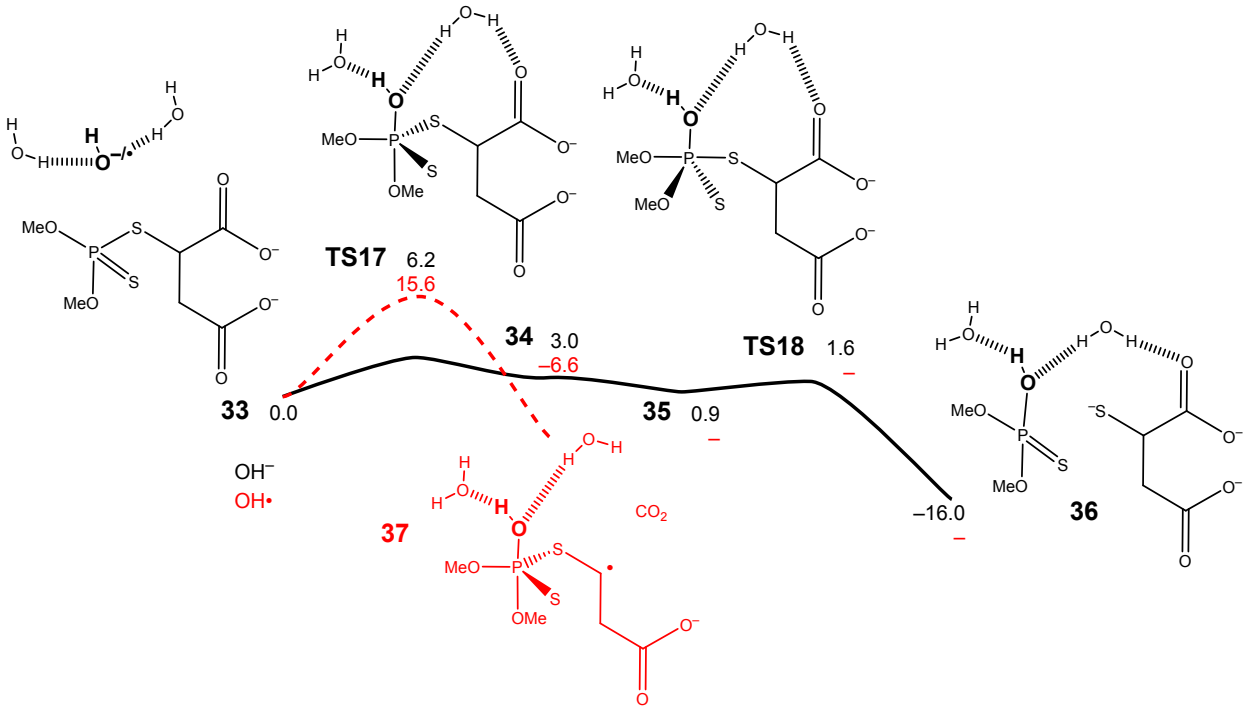

Figure 7. Degradation of P-S bond following ester degradation at the M06-2X/aug-cc-pVTZ//M06-2X/6-31G(d,p) level of theory in bulk water. Non-bolded numbers indicate relative free energies in kcal mol^{-1}. Bolded numbers denote the compound numbers as local minimum (standard) or transition state (leading "TS") geometries. Atoms corresponding to the hydroxide ion or hydroxyl radical are bolded and enlarged throughout the reaction. The position of the negative charge or radical electron are also noted when localized to a single atom.

A similar degradation of the phosphate center is possible with the parent malathion. Although our previous publication indicated this pathway was less likely than ester hydrolysis or elimination, this pathway was still accessible and should therefore be investigated with OH•; these data are shown in Figure 8. Under alkaline conditions, association of the OH^- ion, **TS19**, is accessible and generates the 5-coordinate intermediate **39**. A second step, **TS20**, results in

formation of the thiolate ester and a free phosphate, **40**. However, with OH• radical, the formation of **40** occurs in a single step, **TS21**, with a rather high free energy of activation (19.7 kcal mol^{-1}). Although it is still accessible at room temperature, compared to the previous degradations discussed (*vide supra*) this pathway is not very likely to occur (timescale of 44 s for **TS21** vs 3.66×10^{-5} s for **TS19**).

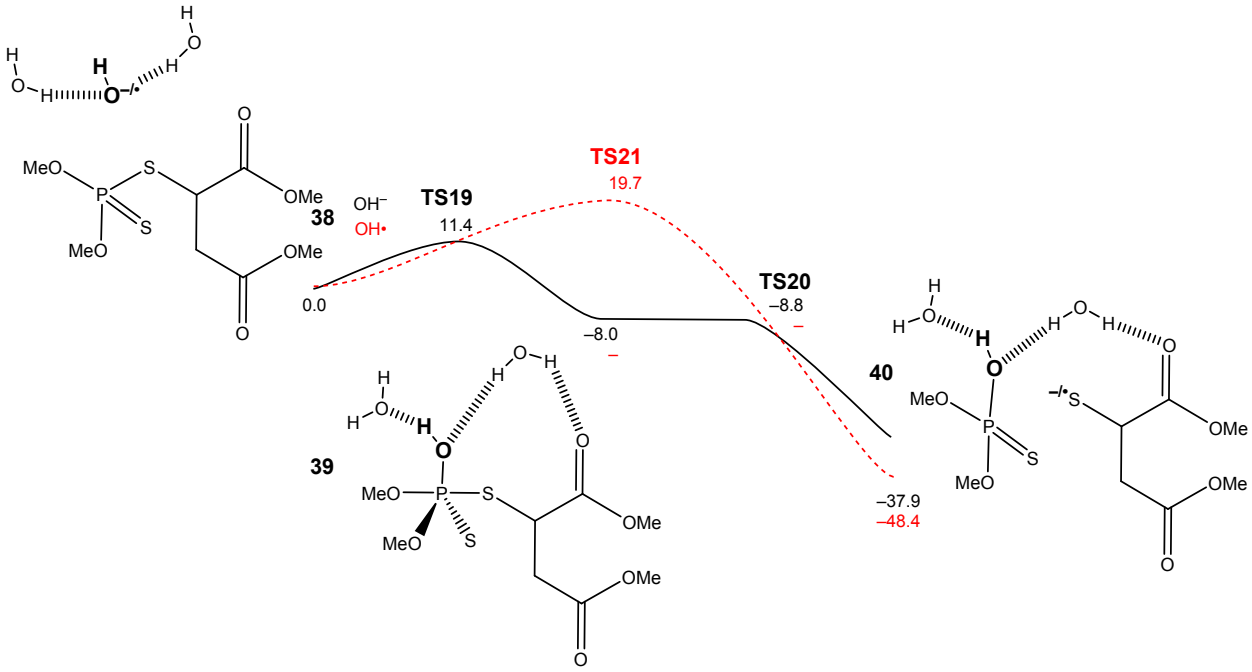

Figure 8. Degradation of P-S bond of malathion at the M06-2X/aug-cc-pVTZ//M06-2X/6-31G(d,p) level of theory in bulk water. Non-bolded numbers indicate relative free energies in kcal mol^{-1}. Bolded numbers denote the compound numbers as local minimum (standard) or transition state (leading "TS") geometries. Atoms corresponding to the hydroxide ion or hydroxyl radical are bolded and enlarged throughout the reaction. The position of the negative charge or radical electron are also noted when localized to a single atom.

Because the OH^- degradation of the P-S bond was still plausible, the subsequent degradation (after dissipation of the byproduct phosphate in **40**) of the ester thiolate with an additional OH• was also investigated; these data are shown in Figure 9. These sequences display similar trends in the ester degradations to those in Figure 5 and Figure 6. With OH^-, the initial association to the α position, **TS22**, is quite low at 4.4 kcal mol^{-1}, but is higher in energy than the subsequent dissociation of methanol, **TS23**, thus indicating that **43** is highly likely to form from **41**. With OH• the association and dissociation trends are similar to OH^-. Although, the initial association, **TS22**, is quite high (22.9 kcal mol^{-1}) and therefore unlikely to occur at room temperature (timescale of 983 s for OH• vs 2.70×10^{-10} s for OH^-). Going one step further, if thiolate ester **41** is first degraded by OH^-, the resulting structure **43** could then exchange the byproduct MeOH for an additional OH^- or OH• and be further degraded. Degradation by OH^- is exergonic and has a moderate free energy of activation for each step (10.4 and 9.6 kcal mol^{-1} for **TS24** and **TS25**). Degradation of the ß position by OH• is more accessible with **TS24** at 16.0 kcal mol^{-1} and thus plausible at room temperature (timescale of 8.61×10^{-2} s), although still notably slower than with OH^- (timescale of 6.76×10^{-6} s). Both the α and ß ester degradations show that with OH^-, the methoxy group dissociates as methanol, whereas with OH• it is lower in energy for the carboxyl group to retain the proton as a carboxylic acid with a proximal OMe•. Although the carboxylic acid is likely to deprotonate once the OMe• migrates away into bulk solution. This trend is similar to the other ester degradations discussed previously.

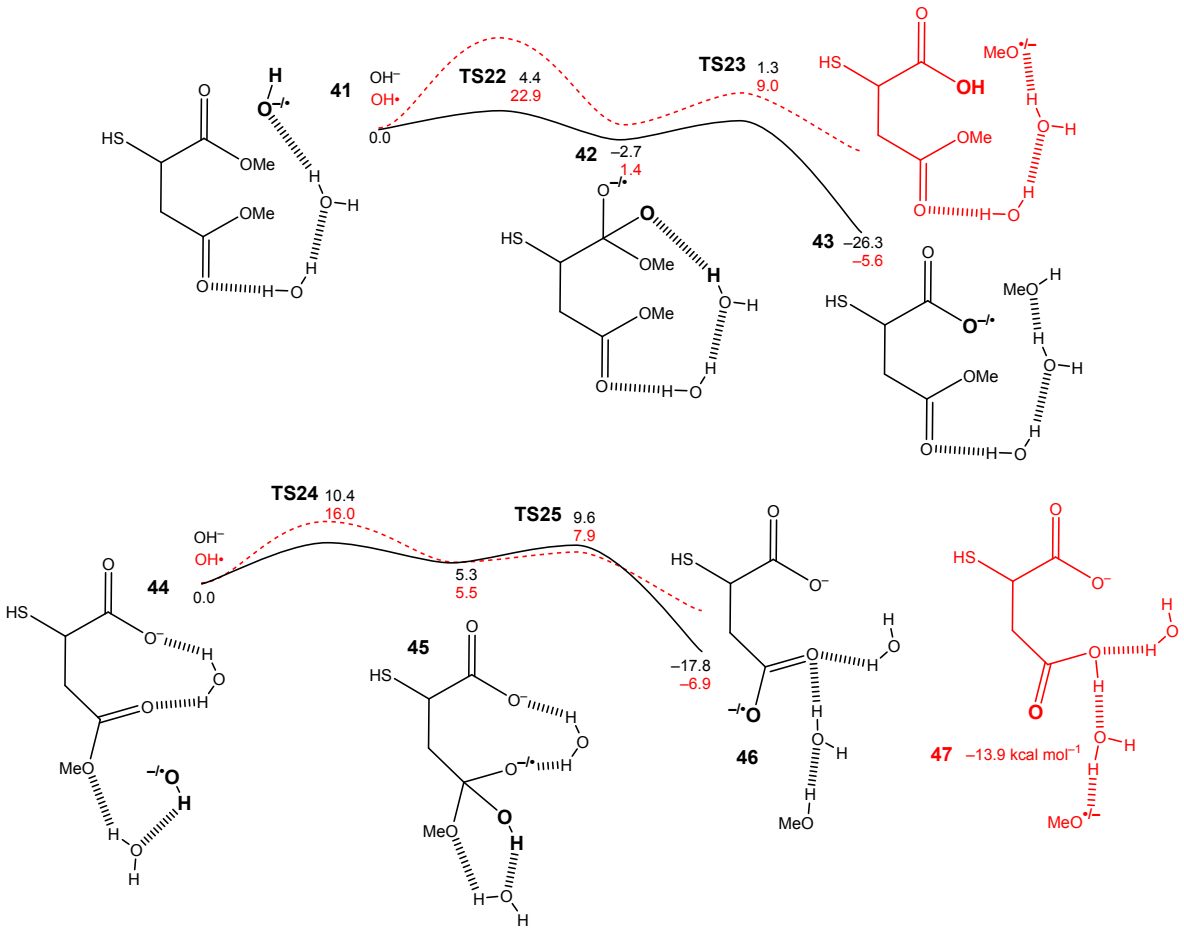

Figure 9. Sequential hydrolysis of the ester groups (α then ß) from the bis-ester thiol at the M06-2X/aug-cc-pVTZ//M06-2X/6-31G(d,p) level of theory in bulk water. Non-bolded numbers indicate relative free energies in kcal mol^{-1}. Bolded numbers denote the compound numbers as local minimum (standard) or transition state (leading "TS") geometries. Atoms corresponding to the hydroxide ion or hydroxyl radical are bolded and enlarged throughout the reaction. The position of the negative charge or radical electron are also noted when localized to a single atom.

CONCLUSIONS

Herein we have compared the various degradation pathways of malathion involving OH^- ion to analogous degradation reactions with OH•. In total, the free energies of activation for the OH^-

ion pathways tend to be lower than the analogous transition states for the OH• pathways, albeit to various degrees. In the case of an elimination type reaction, the two are effectively competitive, whereas for the ester hydrolysis type reactions OH• is still accessible, although significantly, slower. Conversely, OH^- is kinetically incapable of converting fumarate into malate, but this transformation is facile with OH•. Furthermore, once the ester groups have been hydrolyzed from fumarate or malathion, additional OH• radicals further prompt decarboxylation of these compounds thus offering different endpoints to the degradation sequence. These data clearly show that while malathion (and some of its degradation products) can be degraded by either OH• or OH^-, some pathways can be significantly faster or altogether different with OH• than what is available through OH^- alone. These differences in reactivity can potentially be leveraged in multi-step remediation strategies wherein the still toxic by-products from the degradation of the primary contaminant can still be further degraded by changing reagents and/or reaction conditions.

ASSOCIATED CONTENT

Supporting Information.

The following files are available free of charge.

Supplementary Schemes and tabulated energies (PDF)

Molecular coordinates of computed structures (XYZ)

AUTHOR INFORMATION

Corresponding Author

*Manoj.K.Sukla@usace.army.mil

Author Contributions

The manuscript was written through contributions of all authors. All authors have given approval to the final version of the manuscript.

Funding Sources

N/A

ACKNOWLEDGMENT

The use of trade, product, or firm names in this report is for descriptive purposes only and does not imply endorsement by the U.S. Government. The tests described and the resulting data presented herein, unless otherwise noted, were obtained from research funded under the Installations and Operational Environments, Office of the Technical Director of the United States Army Corps of Engineers, and the Environmental Security Technology Certification Program of the Department of Defense by the USAERDC. Permission was granted by the Chief of Engineers to publish this information. The findings of this report are not to be considered as an official Department of the Army position unless so designated by other authorized documents. This work

was supported by a grant of computer time from the DoD High Performance Computing Modernization Program at ERDC, Vicksburg, MS. This document has been approved for public release (Distribution Statement A) by the Engineer Research and Development Center.

REFERENCES

1. F. M. Raushel, Catalytic detoxification, *Nature*, 2011, **469**, 310-311.
2. G. Sankaran, L. Chen, Z. Chen, Y. Liu, T. Lopez, J. Ross, S. Phagura, D. A. Eastmond and R. I. Krieger, The Importance of Hand Exposures to Absorbed Dosage of Hand Harvesters, *Journal of Toxicology and Environmental Health, Part A*, 2015, **78**, 1369-1383.
3. W. E. Cotham and T. F. Bidleman, Degradation of malathion, endosulfan, and fenvalerate in seawater and seawater/sediment microcosms, *Journal of Agricultural and Food Chemistry*, 1989, **37**, 824-828.
4. A. K. Janeczko, E. B. Walters, S. J. Schuldt, M. L. Magnuson, S. A. Willison, L. M. Brown, O. N. Ruiz, D. L. Felker and L. Racz, Fate of malathion and a phosphonic acid in activated sludge with varying solids retention times, *Water Research*, 2014, **57**, 127-139.
5. K. Newhart, Environmental Fate of Malathion.*Journal*, 2006.
6. B. T. Bowman, R. S. Adams and S. W. Fenton, Effect of water upon malathion adsorption onto five montmorillonite systems, *Journal of Agricultural and Food Chemistry*, 1970, **18**, 723-727.
7. L. Lin, M. Xie, Y. Liang, Y. He, G. Y. Sing Chan and T. Luan, Degradation of cypermethrin, malathion and dichlorovos in water and on tea leaves with O3/UV/TiO2 treatment, *Food Control*, 2012, **28**, 374-379.
8. X.-J. Luo, J. Zhao, C.-X. Li, Y.-P. Bai, M. T. Reetz, H.-L. Yu and J.-H. Xu, Combinatorial evolution of phosphotriesterase toward a robust malathion degrader by hierarchical iteration mutagenesis, *Biotechnology and Bioengineering*, 2016, **113**, 2350-2357.
9. S. Kanagasubbulakshmi, R. Kathiresan and K. Kadirvelu, Structure and physiochemical properties based interaction patterns of organophosphorous pesticides with quantum dots: Experimental and theoretical studies, *Colloids and Surfaces A: Physicochemical and Engineering Aspects*, 2018, **549**, 155-163.
10. M. Mehdipour, M. Ansari, M. Pournamdari, L. Zeidabadinejad and M. Kazemipour, Selective extraction of organophosphorous pesticides in plasma by magnetic molecularly imprinted polymers with the aid of computational design, *Analytical Methods*, 2018, **10**, 4136-4142.
11. Y. Liu, S. Liu, Y. Zhang, D. Qin, Z. Zheng, G. Zhu, Y. Lv, Z. Liu, Z. Dong, X. Liao and X. Li, The degradation behaviour, residue distribution, and dietary risk assessment of malathion on vegetables and fruits in China by GC-FPD, *Food Control*, 2020, **107**, 106754.

12. H. Yu, X. Wang, H. Sun and M. Huo, Photocatalytic degradation of malathion in aqueous solution using an Au–Pd–TiO2 nanotube film, *J. Hazard. Mater.*, 2010, **184**, 753-758.
13. F. Matsumura and G. M. Boush, Malathion Degradation by Trichoderma viride and a Pseudomonas Species, *Science*, 1966, **153**, 1278-1280.
14. S. Xie, J. Liu, L. Li and C. Qiao, Biodegradation of malathion by Acinetobacter johnsonii MA19 and optimization of cometabolism substrates, *Journal of Environmental Sciences*, 2009, **21**, 76-82.
15. Y. Vasseghian, M. Moradi, M. Pirsaheb, A. Khataee, S. Rahimi, M. Y. Badi and A. Mousavi Khaneghah, Pesticide decontamination using UV/ferrous-activated persulfate with the aid neuro-fuzzy modeling: A case study of Malathion, *Food Research International*, 2020, **137**, 109557.
16. N. A. Ramos-Delgado, L. Hinojosa-Reyes, I. L. Guzman-Mar, M. A. Gracia-Pinilla and A. Hernández-Ramírez, Synthesis by sol–gel of WO3/TiO2 for solar photocatalytic degradation of malathion pesticide, *Catalysis Today*, 2013, **209**, 35-40.
17. M. I. Swasy, B. R. Brummel, C. Narangoda, M. F. Attia, J. M. Hawk, F. Alexis and D. C. Whitehead, Degradation of pesticides using amine-functionalized cellulose nanocrystals, *RSC Advances*, 2020, **10**, 44312-44322.
18. A. N. Kadam, R. S. Dhabbe, M. R. Kokate, Y. B. Gaikwad and K. M. Garadkar, Preparation of N doped TiO2 via microwave-assisted method and its photocatalytic activity for degradation of Malathion, *Spectrochimica Acta Part A: Molecular and Biomolecular Spectroscopy*, 2014, **133**, 669-676.
19. S. Nasseri, M. Omidvar Borna, A. Esrafili, R. Rezaei Kalantary, B. Kakavandi, M. Sillanpää and A. Asadi, Photocatalytic degradation of malathion using Zn2+-doped TiO2 nanoparticles: statistical analysis and optimization of operating parameters, *Applied Physics A*, 2018, **124**, 175.
20. X. Chai, Y. Cui, W. Xu, L. Kong, Y. Zuo, L. Yuan and W. Chen, Degradation of malathion in the solution of acetyl peroxyborate activated by carbonate: Products, kinetics and mechanism, *Journal of Hazardous Materials*, 2021, **407**, 124808.
21. S. M. Kanan, M. C. Kanan and H. H. Patterson, Photophysical Properties of Ag(I)-exchanged Zeolite A and the Photoassisted Degradation of Malathion, *The Journal of Physical Chemistry B*, 2001, **105**, 7508-7516.
22. R. W. Lamb, H. McAlexander, C. M. Woodley and M. K. Shukla, Towards a comprehensive understanding of malathion degradation: theoretical investigation of degradation pathways and related kinetics under alkaline conditions, *Environmental Science: Processes & Impacts*, 2021, **23**, 1231-1241.
23. M. E. Bender, The toxicity of the hydrolysis and breakdown products of malathion to the fathead minnow (Pimephales Promelas, Rafinesque), *Water Research*, 1969, **3**, 571-582.
24. S. Wang, J. Wang, C. Li, Y. Xu and Z. Wu, Ozone treatment pak choi for the removal of malathion and carbosulfan pesticide residues, *Food Chemistry*, 2021, **337**, 127755.
25. T. J. Nicodemus, C. C. DiRusso, M. Wilson and P. N. Black, Reactive Oxygen Species (ROS) mediated degradation of organophosphate pesticides by the green microalgae Coccomyxa subellipsoidea, *Bioresource Technology Reports*, 2020, **11**, 100461.
26. A. Sudhaik, P. Raizada, S. Thakur, A. K. Saini, P. Singh and A. Hosseini-Bandegharaei, Metal-free photo-activation of peroxymonosulfate using graphene supported graphitic

carbon nitride for enhancing photocatalytic activity, *Materials Letters*, 2020, **277**, 128277.
27. F. De Vleeschouwer, V. Van Speybroeck, M. Waroquier, P. Geerlings and F. De Proft, Electrophilicity and Nucleophilicity Index for Radicals, *Organic Letters*, 2007, **9**, 2721-2724.
28. S. Pari, I. A. Wang, H. Liu and B. M. Wong, Sulfate radical oxidation of aromatic contaminants: a detailed assessment of density functional theory and high-level quantum chemical methods, *Environmental Science: Processes & Impacts*, 2017, **19**, 395-404.
29. M. J. T. Frisch, G. W.; Schlegel, H. B.; Scuseria, G. E.; Robb, M. A.; Cheeseman, J. R.; Scalmani, G.; Barone, V.; Petersson, G. A.; Nakatsuji, H.; Li, X.; Caricato, M.; Marenich, A. V.; Bloino, J.; Janesko, B. G.; Gomperts, R.; Mennucci, B.; Hratchian, H. P.; Ortiz, J. V.; Izmaylov, A. F.; Sonnenberg, J. L.; Williams-Young, D.; Ding, F.; Lipparini, F.; Egidi, F.; Goings, J.; Peng, B.; Petrone, A.; Henderson, T.; Ranasinghe, D.; Zakrzewski, V. G.; Gao, J.; Rega, N.; Zheng, G.; Liang, W.; Hada, M.; Ehara, M.; Toyota, K.; Fukuda, R.; Hasegawa, J.; Ishida, M.; Nakajima, T.; Honda, Y.; Kitao, O.; Nakai, H.; Vreven, T.; Throssell, K.; Montgomery, J. A., Jr.; Peralta, J. E.; Ogliaro, F.; Bearpark, M. J.; Heyd, J. J.; Brothers, E. N.; Kudin, K. N.; Staroverov, V. N.; Keith, T. A.; Kobayashi, R.; Normand, J.; Raghavachari, K.; Rendell, A. P.; Burant, J. C.; Iyengar, S. S.; Tomasi, J.; Cossi, M.; Millam, J. M.; Klene, M.; Adamo, C.; Cammi, R.; Ochterski, J. W.; Martin, R. L.; Morokuma, K.; Farkas, O.; Foresman, J. B.; Fox, D. J., Gaussian 16 C.01.*Journal*, 2016.
30. Y. Zhao and D. G. Truhlar, The M06 suite of density functionals for main group thermochemistry, thermochemical kinetics, noncovalent interactions, excited states, and transition elements: two new functionals and systematic testing of four M06-class functionals and 12 other functionals, *Theoretical Chemistry Accounts*, 2008, **120**, 215-241.
31. M. M. Francl, W. J. Pietro, W. J. Hehre, J. S. Binkley, M. S. Gordon, D. J. DeFrees and J. A. Pople, Self‐consistent molecular orbital methods. XXIII. A polarization‐type basis set for second‐row elements, *J. Chem. Phys.*, 1982, **77**, 3654-3665.
32. M. S. Gordon, J. S. Binkley, J. A. Pople, W. J. Pietro and W. J. Hehre, Self-consistent molecular-orbital methods. 22. Small split-valence basis sets for second-row elements, *Journal of the American Chemical Society*, 1982, **104**, 2797-2803.
33. P. C. Hariharan and J. A. Pople, The influence of polarization functions on molecular orbital hydrogenation energies, *Theoretica chimica acta*, 1973, **28**, 213-222.
34. S. Miertuš, E. Scrocco and J. Tomasi, Electrostatic interaction of a solute with a continuum. A direct utilizaion of AB initio molecular potentials for the prevision of solvent effects, *Chemical Physics*, 1981, **55**, 117-129.
35. S. Miertuš̃ and J. Tomasi, Approximate evaluations of the electrostatic free energy and internal energy changes in solution processes, *Chemical Physics*, 1982, **65**, 239-245.
36. M. Cossi, V. Barone, R. Cammi and J. Tomasi, Ab initio study of solvated molecules: a new implementation of the polarizable continuum model, *Chemical Physics Letters*, 1996, **255**, 327-335.
37. V. Barone, M. Cossi and J. Tomasi, A new definition of cavities for the computation of solvation free energies by the polarizable continuum model, *The Journal of Chemical Physics*, 1997, **107**, 3210-3221.

38. E. Cancès, B. Mennucci and J. Tomasi, A new integral equation formalism for the polarizable continuum model: Theoretical background and applications to isotropic and anisotropic dielectrics, *The Journal of Chemical Physics*, 1997, **107**, 3032-3041.
39. B. Mennucci, E. Cancès and J. Tomasi, Evaluation of Solvent Effects in Isotropic and Anisotropic Dielectrics and in Ionic Solutions with a Unified Integral Equation Method: Theoretical Bases, Computational Implementation, and Numerical Applications, *The Journal of Physical Chemistry B*, 1997, **101**, 10506-10517.
40. B. Mennucci and J. Tomasi, Continuum solvation models: A new approach to the problem of solute's charge distribution and cavity boundaries, *The Journal of Chemical Physics*, 1997, **106**, 5151-5158.
41. V. Barone and M. Cossi, Quantum Calculation of Molecular Energies and Energy Gradients in Solution by a Conductor Solvent Model, *The Journal of Physical Chemistry A*, 1998, **102**, 1995-2001.
42. V. Barone, M. Cossi and J. Tomasi, Geometry optimization of molecular structures in solution by the polarizable continuum model, *Journal of Computational Chemistry*, 1998, **19**, 404-417.
43. M. Cossi, V. Barone, B. Mennucci and J. Tomasi, Ab initio study of ionic solutions by a polarizable continuum dielectric model, *Chemical Physics Letters*, 1998, **286**, 253-260.
44. R. Cammi, B. Mennucci and J. Tomasi, Second-Order Møller−Plesset Analytical Derivatives for the Polarizable Continuum Model Using the Relaxed Density Approach, *The Journal of Physical Chemistry A*, 1999, **103**, 9100-9108.
45. M. Cossi, V. Barone and M. A. Robb, A direct procedure for the evaluation of solvent effects in MC-SCF calculations, *The Journal of Chemical Physics*, 1999, **111**, 5295-5302.
46. J. Tomasi, B. Mennucci and E. Cancès, The IEF version of the PCM solvation method: an overview of a new method addressed to study molecular solutes at the QM ab initio level, *Journal of Molecular Structure: THEOCHEM*, 1999, **464**, 211-226.
47. R. Cammi, B. Mennucci and J. Tomasi, Fast Evaluation of Geometries and Properties of Excited Molecules in Solution: A Tamm-Dancoff Model with Application to 4-Dimethylaminobenzonitrile, *The Journal of Physical Chemistry A*, 2000, **104**, 5631-5637.
48. M. Cossi and V. Barone, Solvent effect on vertical electronic transitions by the polarizable continuum model, *The Journal of Chemical Physics*, 2000, **112**, 2427-2435.
49. M. Cossi and V. Barone, Time-dependent density functional theory for molecules in liquid solutions, *The Journal of Chemical Physics*, 2001, **115**, 4708-4717.
50. M. Cossi, N. Rega, G. Scalmani and V. Barone, Polarizable dielectric model of solvation with inclusion of charge penetration effects, *The Journal of Chemical Physics*, 2001, **114**, 5691-5701.
51. M. Cossi, G. Scalmani, N. Rega and V. Barone, New developments in the polarizable continuum model for quantum mechanical and classical calculations on molecules in solution, *The Journal of Chemical Physics*, 2002, **117**, 43-54.
52. M. Cossi, N. Rega, G. Scalmani and V. Barone, Energies, structures, and electronic properties of molecules in solution with the C-PCM solvation model, *Journal of Computational Chemistry*, 2003, **24**, 669-681.
53. F. Lipparini, G. Scalmani, B. Mennucci, E. Cancès, M. Caricato and M. J. Frisch, A variational formulation of the polarizable continuum model, *The Journal of Chemical Physics*, 2010, **133**, 014106.

54. G. Scalmani and M. J. Frisch, Continuous surface charge polarizable continuum models of solvation. I. General formalism, *The Journal of Chemical Physics*, 2010, **132**, 114110.
55. T. H. D. Jr., Gaussian basis sets for use in correlated molecular calculations. I. The atoms boron through neon and hydrogen, *The Journal of Chemical Physics*, 1989, **90**, 1007-1023.
56. R. A. Kendall, T. H. D. Jr. and R. J. Harrison, Electron affinities of the first - row atoms revisited. Systematic basis sets and wave functions, *The Journal of Chemical Physics*, 1992, **96**, 6796-6806.
57. M. Head-Gordon, J. A. Pople and M. J. Frisch, MP2 energy evaluation by direct methods, *Chemical Physics Letters*, 1988, **153**, 503-506.
58. S. Sæbø and J. Almlöf, Avoiding the integral storage bottleneck in LCAO calculations of electron correlation, *Chemical Physics Letters*, 1989, **154**, 83-89.
59. M. J. Frisch, M. Head-Gordon and J. A. Pople, A direct MP2 gradient method, *Chemical Physics Letters*, 1990, **166**, 275-280.
60. M. J. Frisch, M. Head-Gordon and J. A. Pople, Semi-direct algorithms for the MP2 energy and gradient, *Chemical Physics Letters*, 1990, **166**, 281-289.
61. M. Head-Gordon and T. Head-Gordon, Analytic MP2 frequencies without fifth-order storage. Theory and application to bifurcated hydrogen bonds in the water hexamer, *Chemical Physics Letters*, 1994, **220**, 122-128.
62. Z. A. Ali, F. W. Aquino and B. M. Wong, The diamine cation is not a chemical example where density functional theory fails, *Nature Communications*, 2018, **9**, 1-3.
63. N. L. Wolfe, R. G. Zepp, J. A. Gordon, G. L. Baughman and D. M. Cline, Kinetics of chemical degradation of malathion in water, *Environmental Science & Technology*, 1977, **11**, 88-93.